On the problem of local tissue hyperthermia control: multiscale modelling of pulsed laser radiation action on a medium with embedded nanoparticles

Yu.A. Avetisyan, A.N. Yakunin, V.V. Tuchin

Abstract. **Methods for solving analytically and numerically the problem of multiscale modelling of the laser hyperthermia processes in a medium with nanoparticles are developed with regard to composite spherical nanoparticles (nanoshells). The features of the laser radiation field localisation on nanoscale inhomogeneities are investigated. Issues related to the control of the tissue hyperthermia processes by choosing the parameters of spatiotemporal localisation of the laser beam and of the absorbing nanoparticles are discussed.**

Keywords: *time-dependent temperature field modelling, laser hyperthermia, composite nanoparticles.*

1. Introduction

Laser therapy belongs to the promising areas of modern medicine. In many cases the therapeutic effect of laser radiation is inseparably linked with the process of tissue hyperthermia, which may be a principal effect as well as a concomitant one [1 – 3]. The development of models for calculating the temperature field of the tissue exposed to laser radiation made it possible to carry out investigations, basing on which the methods of hyperthermia have been proposed and justified not only for surface but also for subcutaneous layers of biotissue [1, 4, 5]. However, an essential disadvantage of currently used techniques of cancer hyperthermia is their limited selectivity and low spatial resolution. This implies that, when heating the cancer, the undesired heating of a considerable area of surrounding healthy tissue simultaneously occurs.

One of the novel and efficient methods of localisation of external and internal heat generation areas is photothermal labelling of a cancer tumour with gold nanoparticles of various shape and structure, e.g., nanoshells, nanorods, nanocells, etc. [6 – 14]. In this case, due to the strong absorption of laser radiation by nanoparticles in certain spectral regions (referred to as the plasmon resonance absorption), cells labelled with these particles are locally and selectively heated, which substantially reduces the probability of undesired injuring of a healthy surrounding tissue.

It should be noted, that in this case the sizes of absorbing particles and, therefore, the degree of heat load localisation, are as large as tens of nanometres. The necessity to solve the problem simultaneously for macroscopic (millimetre and tens of millimetres) and microscopic (fractions of a micrometer) objects makes the existing models of temperature field calculation unacceptable for practical use and providing efficient control of hyperthermia processes.

Generally, the interaction of radiation with a biological tissue containing absorbing nanoparticles is a rather complex process having multiple aspects (see, e.g., [3, 6, 7]). Strong scattering by the biotissue itself essentially transforms the characteristics of the probing light. Thus, for a picosecond or smaller duration of the illuminating pulse, inside the biotissue the pulse duration increases up to nanoseconds [3], and a near-isotropic angular distribution of the scattered light intensity can settle down (the so-called diffusion regime [3]).

The analysis of the kinetics of temperature fields, additionally arising in the biotissue when doped with absorbing nanoparticles, is also nontrivial. For very small particles (with characteristic size less than 10 nm, see below) the optical and thermal characteristics can no longer be determined by extrapolation of data for bulk samples of the corresponding materials and should be found with quantum-mechanical calculations. Moreover, the consideration of fast thermal processes in a condensed medium requires separate analysis of the temperature dynamics for the electrons and the crystal lattice of the sample.

Naturally, the formulation of specific recommendations for clinical practice requires performing a variety of studies, namely, modelling the hyperthermia in a biological tissue, containing absorbing nanoparticles, with all above-mentioned factors taken into account and careful testing of the results, basing on the comparison with the data of experiments and subsequent preclinical trials. In the present paper, focusing the attention on the calculation technique within the framework of the two-scale approach developed (calculation of both the locally averaged temperature field and the temperature gradients within the individual nanoparticles and in their immediate proximity), we deliberately divert our attention away from the rigorous account for some of above-mentioned factors, using the following simplifications.

Yu.A. Avetisyan, A.N. Yakunin Institute for Problems of Precision Mechanics and Control, Russian Academy of Sciences, ul. Rabochaya 24, 410028 Saratov, Russia; e-mail: yuavetisyan@mail.ru, anyakunin@mail.ru;
V.V. Tuchin Institute of Precision Mechanics and Control, Russian Academy of Sciences, ul. Rabochaya 24, 410028 Saratov, Russia; N.G. Chernyshevsky Saratov State University, ul. Astrakhanskaya 83, 410012 Saratov, Russia; e-mail: tuchinvv@mail.ru

We restrict our consideration to the analysis of relatively long illuminating pulses (not less than nanosecond duration), acting on the nanoparticles with the typical size noticeably larger than 10 nm. As justified in Ref. [15], the calculation of optical characteristics of such particles still does not require the involvement of the quantum-mechanical approach, and these characteristics appear to be close to those of bulk samples, with proper correction for plasmon resonance absorption [16], for which the heating dynamics is quite satisfactorily described by the common classical heat conduction equation (without separate consideration of the temperatures of electron and crystal lattice fractions), as demonstrated in [11]. Finally, for simplicity we neglect the scattering properties of the medium, surrounding the nanoparticles. The light field in the medium is modelled with a locally plane electromagnetic wave, which allows one to visualise the heat source distribution details in the composite nanoparticles under consideration.

Note, that due to the linearity of the optical part of the problem considered, the account for the scattering of radiation by the medium would, in fact, be reduced to the summation of a continuum of such plane waves, acting on a nanoparticle, with a given angle distribution of their intensities. This distribution (close to an isotropic one in the diffusion regime of scattering) may be found using known methods (see, e.g., [3–5]). In addition, by choosing the duration of the heating pulses in the nanosecond range, we substantially account for the influence of tissue scattering properties on the propagating pulse, which, whatever short initially, appears within the tissue already 'broadened', and for tissues as thick as a few centimeters such 'broadening' amounts to a few nanoseconds.

The present paper is devoted to further development of methods for solving analytically and numerically the problem of multiscale modelling of the laser hyperthermia process in a medium, containing nanoscale particles [13, 14, 17], with regard to composite spherical nanoparticles (nanoshells). The features of the laser radiation field localisation at nanoscale inhomogeneities and the corresponding distributions of the thermal loss density are studied and the time-dependent temperature fields under the irradiation in the pulsed regime are calculated. The factors that cause the need for using a multiscale approach to provide reliable control of the spatial distribution of the temperature field both inside the absorbing nanoparticles and in the surrounding medium are determined.

2. Mathematical formulation of the problem

In correspondence with the approximations assumed, we considered an ensemble of nanoparticles, embedded in an optically isotropic and homogeneous substance, irradiated with laser light. The thermal field, arising in such a system, was modelled using the solution of the time-dependent heat conduction equation (see, e.g., [3, 18])

$$c\rho \frac{\partial T}{\partial t} = \mathrm{div}(k\,\mathrm{grad}\,T) + Q. \qquad (1)$$

Here, c, ρ, and k and are the local values of the specific heat, density, and heat conductivity coefficient, respectively; T is the temperature; t is the time; $Q = \omega\varepsilon''|E|^2(8\pi)^{-1}$ is the intensity of the heat sources due to the absorption of

radiation [19], averaged over the period of the optical field oscillation; ω and E are the circular frequency and the local value of the electric field amplitude; ε'' is the imaginary part of the medium permittivity.

Direct solution of Eqn (1) with appropriate boundary and initial conditions for a macroscopically large number of nanoparticles is a matter of significant mathematical difficulties. The problem is complicated by sharp drops of the optical and thermal characteristics, observed at the nanoparticle – surrounding medium interface and within the nanoparticles (the latter is typical, particularly, of nanoshells). In connection with this, we applied the approach, analogous to that used in [8] for the analysis of the thermal field in a system of nanorods. Namely, first we average Eqn (1) over physically small volumes. The solution of the resulting equation allows one to study the kinetics of the medium heating in a practically interesting case of a macroscopically large number of nanoparticles. However, as discussed above, in this case the information about the small-scale inhomogeneity of the heating is lost. To remove this defect, we estimated the kinetics of temperature gradients both within the nanoparticles and in the surrounding medium using the solution of Eqn (1) for a single nanoshell at different durations of the irradiating pulse.

The model of a distributed medium (macroscale modelling). Under the typical experimental conditions [6, 7] the suspensions of nanoparticles with small concentrations $N_0 \sim 10^9 - 10^{10}$ cm^{-3} were used. In this case one can assume that the thermal characteristics (c, ρ, k) of such a composite medium coincide with those of a medium without nanoparticles. As before, the kinetics of the thermal field will be described by Eqn (1), in which, however, T and Q should be understood not as exact local values of the temperature and the intensity of heat sources, but as the values of these variables, averaged over physically small volumes, containing, at the same time, a sufficiently large number of nanoparticles.

The model for calculating the small-scale inhomogeneity of the temperature field (microscale modelling). At small concentrations N_0 of nanoparticles, the mean distance between them $(\sim N_0^{-1/3} \approx 10^4$ nm) considerably exceeds their characteristic size $\sim 10^2$ nm [6, 7]. In this case, the small-scale inhomogeneity of the temperature field can be estimated using the solution of Eqn (1) for a single particle. Naturally, in contrast to the distributed medium model, now it is necessary to account not only for the thermal characteristics of the surrounding medium (c_m, ρ_m, k_m) but also for those of the nanoparticle itself. The latter was considered to be a nanoshell with the core made of fused silica (thermal characteristics c_1, ρ_1, k_1) covered with gold (c_2, ρ_2, k_2). The solution of Eqn (1) should satisfy the conditions of continuity for the temperature T and the heat flow $-k\,\mathrm{grad}\,T$ at the interface between the media.

3. Results of the modelling

3.1 Analytical solution of the model macroscopic level problem

First we considered a simplified distributed medium model, assuming that the absorbing nanoparticles localised in a certain volume V are imbedded in an infinite nonabsorptive medium. Then, for an arbitrary spatiotemporal dependence

of the absorption $Q(\boldsymbol{r}, t)$, the solution of Eqn (1) may be written in the form (see, e.g., [18])

$$T(\boldsymbol{r}, t) = T_0 + \int_V \mathrm{d}^3 \boldsymbol{r}' \int_0^t \mathrm{d}t' \frac{Q(\boldsymbol{r}', t')}{c\rho \left[2a\sqrt{\pi(t - t')}\right]^3}$$

$$\times \exp\left[-\frac{|\boldsymbol{r} - \boldsymbol{r}'|^2}{4a^2(t - t')}\right]. \tag{2}$$

It is assumed here that at the initial moment of time $t = 0$, the temperature at all points has the same value T_0; $a^2 \equiv k/(c\rho)$ being the thermal diffusivity of the medium.

Considering a rectangular irradiating pulse with the duration t_p which is by many orders of magnitude higher than the period of the optical field oscillation $\sim 1/\omega$, and neglecting the spatial inhomogeneity of the radiation absorption in the whole volume V, we will use the approximation: $Q(\boldsymbol{r}, t) = Q_0$ at $0 < t \leqslant t_\mathrm{p}$ and $Q(\boldsymbol{r}, t) = 0$ at $t > t_\mathrm{p}$. And, finally, for simplicity let us consider the volume V to have the shape of a sphere with the radius R.

The simplifications accepted allow one to perform analytically the necessary integration in Eqn (2). As a result, the sought-for temperature appears to be dependent only on the distance r from the centre of the sphere and on the time t:

$$T(r, 0 < t \leqslant t_\mathrm{p}) = T_0 + \frac{Q_0 R^2}{2k}$$

$$\times \left[1 - \frac{1}{3}u^2 + \Phi(u_-, t) - \Phi(u_+, t)\right] \quad \text{for} \quad 0 < u \equiv \frac{r}{R} < 1,$$

$$T(r, 0 < t \leqslant t_\mathrm{p}) = T_0 + \frac{Q_0 R^2}{2k} \tag{3}$$

$$\times \left[\frac{2}{3}\frac{1}{u} + \Phi(u_-, t) - \Phi(u_+, t)\right] \quad \text{for} \quad u \equiv \frac{r}{R} \geqslant 1,$$

where $u_\pm \equiv u \pm 1$,

$$\Phi(u_\pm, t) \equiv \mathrm{erf}(BRu_\pm)\left[\frac{1}{3}\frac{u_\pm^3}{u} - \frac{1}{2}u_\pm^2 - \frac{1}{4(BR)^2}\right] + \frac{1}{BR\sqrt{\pi}}$$

$$\times \exp\left[-(BRu_\pm)^2\right]\left[\frac{1}{3}\frac{u_\pm^2}{u} - \frac{1}{2}u_\pm - \frac{1}{6(BR)^2 u}\right]; \tag{4}$$

$$B \equiv \frac{1}{2a\sqrt{t}}; \quad \mathrm{erf}(\xi) = \frac{2}{\sqrt{\pi}}\int_0^\xi \exp\left(-x^2\right)\mathrm{d}x$$

is the error integral. Here, we restricted ourselves to writing down the form of the solution in the most interesting region $0 < t \leqslant t_\mathrm{p}$, while at $t > t_\mathrm{p}$ the solution quickly decays (Fig. 1). The character of the obtained solution is partially displayed in Figs 1 and 2.

It was assumed in the calculations that in the transparent medium with the refractive index $n_\mathrm{m} = 1.33$, far from the boundaries of the medium there is a spherical absorptive region with the radius $R = 0.5$ cm, homogeneously filled with nanoparticles with the concentration $N_0 = 5 \times 10^9$ cm^{-3}. As in the experiments [6, 7], these particles are nanoshells with a fused silica core (with the refractive index $n_1 = 1.46$ and the radius $R_1 = 70$ nm), coated with a gold layer (with the refractive index $n_2 = 0.15 + \mathrm{i}4.64$ and the
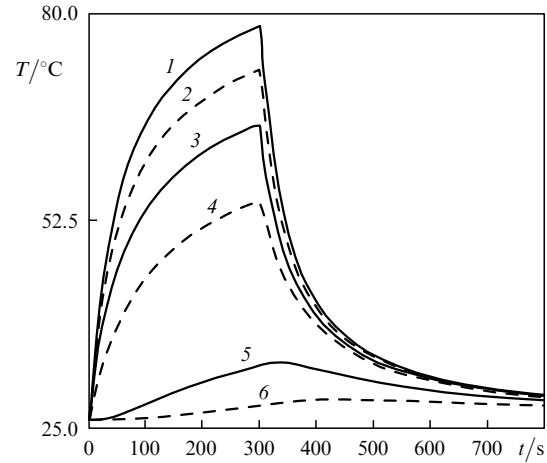

Figure 1. Kinetics of heating of a spherical volume ($R = 0.5$ cm) of localisation of nanoscale particles ($1-4$) and the surrounding medium ($5, 6$) under the action of a rectangular radiation pulse with the intensity 4 W cm^{-2} and duration 300 s at the distance $r = 0$ (1), $0.5R$ (2), $0.75R$ (3), R (4), $2R$ (5), and $3R$ (6) from the centre of the localisation volume.

layer thickness $\delta = 20$ nm, so that the total radius of the core with the coating is $R_2 = 90$ nm). At the initial moment of time, the medium with nanoparticles has the temperature $T_0 = 26$ °C and is irradiated by a rectangular laser pulse having the intensity $I = 4$ W cm^{-2} and the duration $t_\mathrm{p} = 300$ s. The laser radiation wavelength is $\lambda = 800$ nm. The following thermal characteristics of the medium were used: $c = 4182$ J kg^{-1} deg^{-1}, $\rho = 10^3$ kg m^{-3}, $k = 0.6$ W deg^{-1} m^{-1}. In correspondence with the considered approximation of a distributed medium, the intensity of heat sources is averaged over the physically small volume:

$$Q = 2\pi\tau N_0 V_\mathrm{cov} \varepsilon_2'' \langle \beta \rangle I/\lambda. \tag{5}$$

Here, $\tau \equiv |E_\mathrm{m}|^2/|E_0|^2$ is the transmission coefficient of the medium, surrounding the nanoparticles, onto which the laser beam (approximated by a plane linearly polarised wave with the complex amplitude E_0) is incident from the vacuum; E_m is the complex amplitude of the light in the medium; $\varepsilon_2 \equiv n_2^2$ and ε_2'' is the dielectric constant of the gold coating and its imaginary part, respectively; the dimensionless coefficient

$$\langle \beta \rangle \equiv V_\mathrm{cov}^{-1} \int_{V_\mathrm{cov}} \mathrm{d}^3 \boldsymbol{r} \beta$$

is the quantity $\beta \equiv |E_2|^2/|E_\mathrm{m}|^2$, averaged over the volume of the nanoparticle coating $V_\mathrm{cov} = 4\pi(R_2^3 - R_1^3)/3$ and proportional to the ratio of the energy density of the electric field, diffracted into the shell of the nanoparticle, to that of the irradiating field in the medium; E_2 is the vector complex amplitude of the electric field in the corresponding region. We should note, that, first, in Eqn (5) only single scattering of the irradiating light by the ensemble of nanoparticles is taken into account, and only the golden coating is assumed to absorb radiation. Second, together with the quantity E_2, the parameter β appears to be spatially inhomogeneous, which is discussed at the end of the present subsection. Third, the expressions obtained for the quantities β and $\langle \beta \rangle$

as a result of the calculation of the diffraction of a plane wave on the nanoshells in the quasi-electrostatic approximation (see, e.g., [15]), are presented in Appendix. Finally, the Fresnel transmission coefficient $4/(1 + n_m)^2$ was used for τ.

Thus, the essential inhomogeneity of heating of both the region, where the absorption of radiation occurs, and the surrounding medium is apparent (Fig. 1). Note that all dependences are obtained in a relatively simple analytical form and satisfactorily agree with appropriate experimental curves presented in Refs [6, 7] (see, in particular, Fig. 5 from Ref. [6]). The temperature distribution, which appears to be maximal at the centre of the radiation-absorbing region, has the simplest form in the steady-state regime. Such a regime is implemented at pulse durations $t_p \gg R^2/(4a^2)$ in the interval $t_p > t \gg R^2/(4a^2)$, when the contribution of the functions $\Phi(u_\pm, t)$, describing the transient behaviour, appears to be inessential in Eqn (3).

The corresponding illustration is presented in Fig 2 for the steady-state distributions of the temperature T and of the magnitude of the heat flow density $|J| = |-k\nabla T|$. Thus, in Fig. 2 the radial temperature distribution inside the sphere $(0 \leqslant r \leqslant R)$ is described by a parabolic law. At the boundary of the absorbing region, the excess of the temperature over its initial value $T_0 = 26\,°C$ amounts to 2/3 of the corresponding excess at the centre. Outside the sphere $(r > R)$, with the growth of r the temperature decreases following a hyperbolic law (Fig. 2a). Correspondingly, the heat flow density grows linearly inside the sphere and decreases as $\sim 1/r^2$ outside it (Fig. 2b). The efficiency of the light energy conversion into heat in the steady state may be characterised by the ratio of the heat flow density at the boundary to the intensity of irradiating light. Then for the case under consideration this value is $\sim 14\,\%$ (Fig. 2b).

Consider now the radiation absorption within the golden shell of a separate nanoparticle, which will be used in Subsection 3.3 for the analysis of temperature gradients in the framework of the microscale approach. In this case, the local intensity of heat sources may be presented in the form

Figure 2. Spatial steady-state distribution of the temperature T (a) and the magnitude of the heat flow density $|J|$ (b) for the absorbing medium whose parameters are presented in Fig. 1.

$$Q_1 = 2\pi\tau\varepsilon_2''\beta I/\lambda. \tag{6}$$

The results of calculation using Eqn (6) for linearly polarised irradiating light are partially presented in Fig. 3. Alongside with the axial symmetry of the picture (no dependence on the azimuthal angle φ), the pronounced inhomogeneity of the light absorption is clearly seen both across the shell thickness [curves $(1-3)$] and, particularly, with respect to the polar angle, namely, the absorption is maximal at the 'equator' (at $\theta = 90°$) and is practically zero at the 'poles' (at $\theta = 0$ and $\theta = 180°$). This angular dependence can be also easily seen directly from the expression for β given in Appendix in the case $|\varepsilon_2| \gg |\varepsilon_1|, |\varepsilon_m|$, considered here, for relatively thin shells $(R_2 - R_1 \ll R_1)$, when a rough estimate yields $Q_1(\theta) \sim \sin^2\theta$ [see Eqn (A.2)].
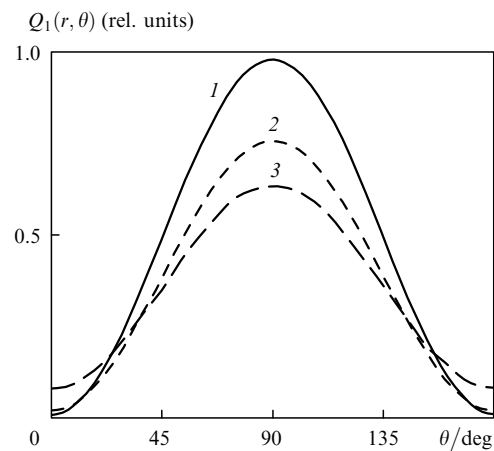

Figure 3. Distribution of the local intensity of heat sources in a spherical nanoshell at the distance $r = R_1$ (1), $r = (R_1 + R_2)/2$ (2), and $r = R_2$ (3) from its centre versus the polar angle θ between the polarisation vector of the irradiating light and the direction vector pointing at the observation point. The geometrical and optical characteristics of the nanoshell have the same values as above.
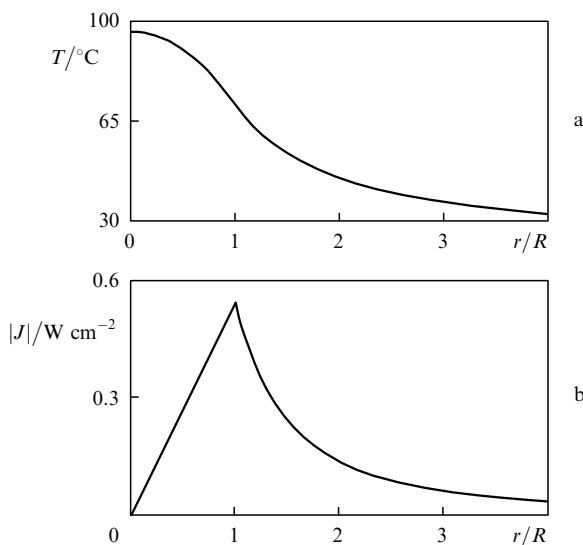
Thus, the analysis of temperature gradients in nanoshells with the considered structure and in the surrounding medium generally requires accounting for the spatial inhomogeneity of the local intensity of heat sources within these shells, mentioned above. We plan the implementation of such an improved analysis for the future, whereas in Subsection 3.3 of the present paper we, for simplicity, restrict ourselves to considering the intensity of thermal sources within the nanoshells to be constant:

$$\langle Q_1 \rangle = 2\pi\tau\varepsilon_2''\langle\beta\rangle I/\lambda, \tag{7}$$

where the expression for $\langle\beta\rangle$ is given in Appendix.

3.2 Finite-element macroscale modelling of heating the biotissue with absorbing nanoparticles

We proceed to considering a more general case, when the region where nanoparticles are localised has the shape of an ellipsoid of revolution with the major axis of 15 mm and the minor axes of 10 mm, one of the latter being coincident with the axis of the laser beam (z axis). The heat conduction equation (1) is solved by the finite-element method using the bundled software COMSOL [20]. Again, only the
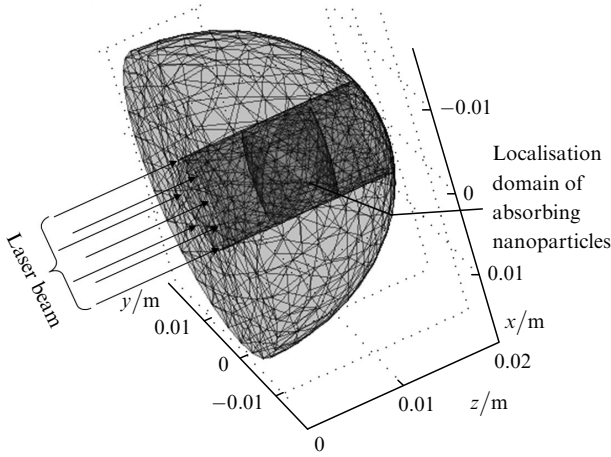
Figure 4. Three-dimensional finite-element grid in the calculation domain. The grid spacing is smaller in the zone of laser beam propagation; the grid is additionally condenced in the region of absorbing nanoparticles injection to reduce the numerical computation error [17].

Figure 6. Distribution kinetics of the temperature T_1 along the axis of the laser beam irradiating a medium with nanoparticles.

Figure 7. Change in the temperature T_1 in the calculation domain with the maximal temperature as a function of the dimensionless time normalised to the exposure time $t_0 = 300$ s.

radiation absorption by the nanoparticles appearing in the laser beam is taken into account. It is assumed that the heat generation in the biotissue free of nanoparticles is negligible. The shape of the calculation domain (geometrical model) and its finite-element discretization are illustrated in Fig. 4.

The adiabatic boundary condition $\partial T_1/\partial n|_{S_1} = 0$ is imposed on the solution at the outside plane surface S_1 of the medium, through which the laser irradiation is introduced, where $T_1 = T - T_0$; T_0 is the temperature of the medium in the unperturbed region (far from heat sources); n is the normal vector to the surface S_1. At the rest part S_2 of the calculation domain surface the boundary condition is $T_1|_{S_2} = 0$. The initial condition at $t = 0$ in the calculation domain V is taken to have the form $T_1|_V = 0$. The calculation results of the time-dependent temperature field are shown in Figs 5–7.
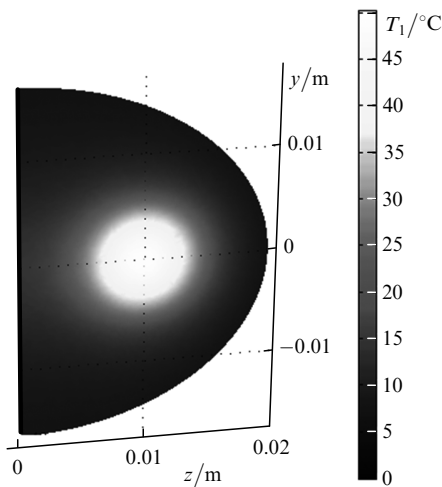

Figure 5. Distribution of temperature T_1 in the longitudinal sectional view of the macroscopic calculation domain (passing through the beam axis z) at the moment of time $t = 300$ s, corresponding to the end of light exposure. The maximal temperature is $T_1^{max} = 50.3\,°C$. The zero of the image grayscale corresponds to the temperature $T_0 = 26\,°C$.
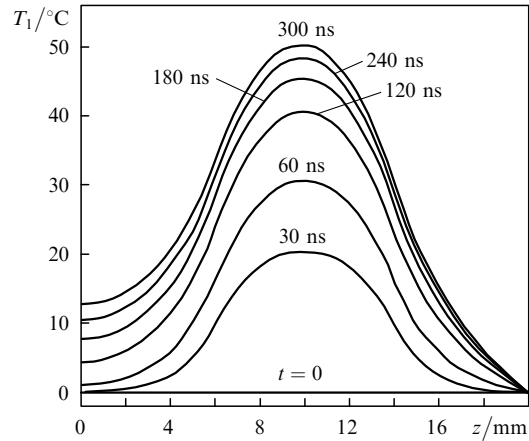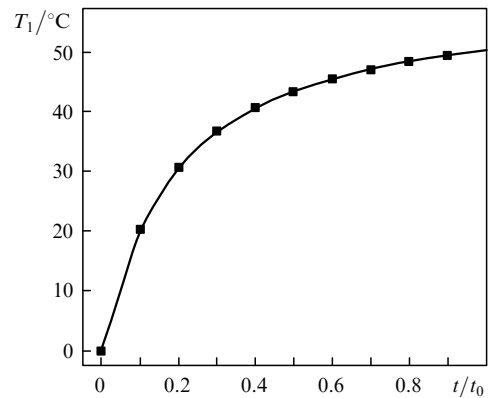
The analysis of the obtained numerical results allows one to conclude that they agree quite well with the kinetics of the temperature variations, observed experimentally [6, 7] in the medium with nanoparticles, irradiated with a laser beam. The fast growth of the temperature at the beginning of the exposure time substantially slows down during the subsequent 1–2 minutes. Approaching a steady state occurs with the rates of the temperature growth of the order of a few Celsius degrees per minute or less. As the estimates show, the steadying of the temperature at the assumed parameters of the laser beam and the concentration of nanoparticles may take a few tens of minutes.

At the same time, it may be seen from Figs 5 and 6 that the temperature field in the region of localisation of nanoparticles, irradiated with the laser beam, is characterised by a considerable spatial inhomogeneity (in the interval 5 mm < z < 15 mm at the end of the exposure time the temperature drop approaches 18 °C). This effect should be necessarily taken into account when estimating the influence of hyperthermia or thermolysis on a tissue and choosing the exposure duration. Obviously, the reduction of the spatial inhomogeneity of the temperature field in the region of nanoparticle injection would improve the possibility to control hyperthermia and photothermolysis and make the influence of different factors less critical when determining the exposure duration. The potential possibilities to control the laser beam action on the medium can be enhanced by

using a pulsed regime instead of a cw one. The features of tissue heating in pulsed regime are considered below.

3.3 Finite-element microscale modelling of heating the medium with absorbing nanoparticles

In correspondence with the approach described above, the microscale modelling is used to account for the local gradients of the temperature T_2 arising due to the inhomogeneity of local heat generation in the nanoshells, absorbing the electromagnetic radiation. In spite of a substantial thermal resistance of the layer, surrounding an individual particle (its thickness depending on the concentration of nanoparticles and typically having the order of $10^3 - 10^4$ nm [3, 8]), the temperature gradient as such is caused both by the specific heat load density in the nanoparticle shell and by the medium inertia (thermal conductivity parameters).

Figure 8 presents the results of calculation of local variations in the temperature T_2 (the increments of temperature during the laser pulse) in the microscopic domain 'nanoparticle and its neighbourhood' as a function of the pump pulse duration and the laser beam intensity, provided that the magnitude of the heat pulse (i.e., the amount of heat energy) is constant. The geometrical parameters of the composite nanoparticles and the thermal properties of the medium are given in Subsection 3.1. The following thermal parameters were used: $k_1 = 1.4$ W m^{-1} K^{-1}, $_1 = 2400$ J kg^{-1} K^{-1}, $\rho_1 = 2200$ kg m^{-3} for the fused silica core and $k_2 = 300$ W m^{-1} K^{-1}, $c_2 = 130$ J kg^{-1} K^{-1}, $\rho_2 = 19300$ kg m^{-3} for the golden shell. The size of the finite elements for the discretization of the calculation domain is not less than 0.1 of the thickness of the golden shell, in which the heat generation occurs; the volume of the calculation domain is two orders of magnitude larger than the volume of a nanoparticle.
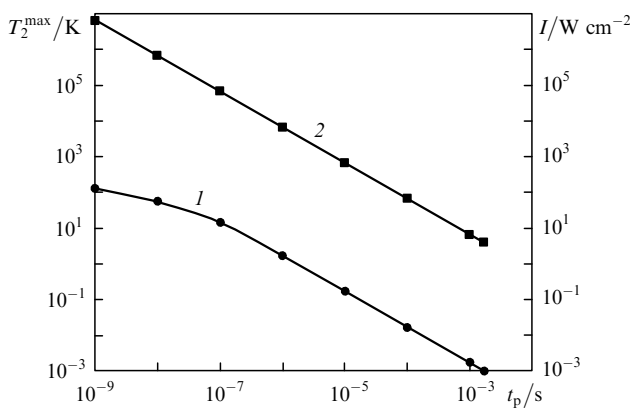

Figure 8. The maximal temperature increment T_2^{max} in the microscopic domain 'nanoparticle and its neighbourhood' (_1_) and the intensity of the laser beam _I_, providing the same magnitude of the heat pulse (_2_), versus the pump pulse duration.

Though, in correspondence with curve (_2_) in Fig. 8, the reduction of the pulse duration with a simultaneous increase in the intensity _I_ does not change the amount of the thermal energy, generated in the nanoparticle per pulse, no temperature equivalence of the regimes is observed, namely, the amount of the additional temperature increment T_2^{max} in the vicinity of the nanoparticle considerably grows, as seen from curve (_1_) in Fig. 8. If the additional increase in the

temperature by 1 °C due to fast processes of heating and relaxation under the pump pulse action is taken to be a significance test, the pulse duration of 10 μs will be a landmark, as follows from curve (_1_). Curve (_2_) in Fig. 8 allows one to determine the intensity _I_ of the laser beam, corresponding to this duration ($I \sim 1$ kW cm^{-2}). At the pulse duration 2 ns and the intensity $I = 5$ MW cm^{-2}, the increment T_2 reaches already 100 °C, etc.

From the results of our calculations we conclude that a drastic reduction of the magnitude of thermal pulses is possible when using nanosecond pulse regimes of laser irradiation that provide the required level of hyperthermia. In this case, the inhomogeneity of the temperature distribution in the irradiation zone, caused by macroscopic diffusion processes and considered in the previous two subsections, can be minimised. Simultaneously, the zone of undesired overheating of the healthy tissue is reduced. These factors indicate that the effect of the absorbed laser radiation power localisation may have promising applications.

The results of calculation of the temperature field, presented in Figs 9 and 10, allow one to estimate the spatiotemporal parameters of transient thermal processes in a composite nanoparticle and in its vicinity.
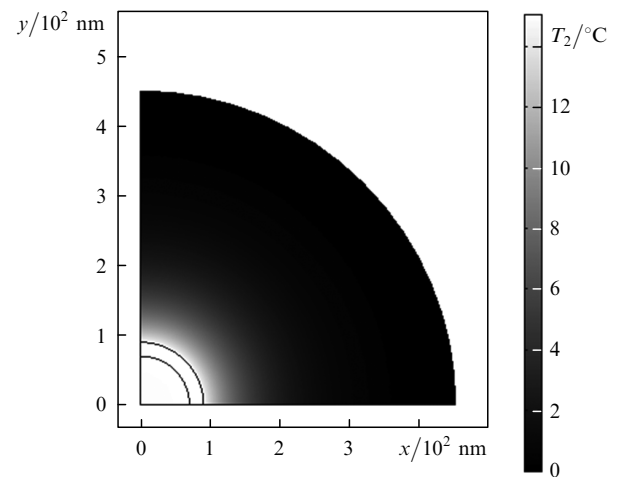

Figure 9. Distribution of the temperature increment T_2 in the microscopic domain 'golden nanoshell and its neighbourhood' at the end of the 100-ns pump pulse under the action of the irradiating laser beam with the intensity $I = 100$ kW cm^{-2}. (Due to the distribution symmetry, we consider one quarter of the cross section of the spherical microscopic domain; the points with $0 \leqslant r < 70$ nm lie in the core, $70 \leqslant r \leqslant 90$ nm in the shell, and $90 < r \leqslant 450$ nm in the microscopic domain of the medium, surrounding the nanoparticle.) The maximal temperature is $T_2^{max} = 15$ °C.

At the onset of the pump pulse, a minimum of the temperature T_2 is observed in the central part of the nanoparticle core (Fig. 10, lower curves). At the end of the pulse, this minimum vanishes, and the temperature within the entire core becomes practically equal to that of the golden shell (upper curves in Fig. 10 and the distribution of T_2 in Fig. 9).

The cause of such a behaviour is that the finite heat-flow velocity in the core material (characterised by thermal diffusivity [21]) and the core size determine the limiting pulse duration t_p^{lim}, above which the temperature gradients inside the core of the composite nanoparticle can be neglected (the heat energy of the pulse being constant).
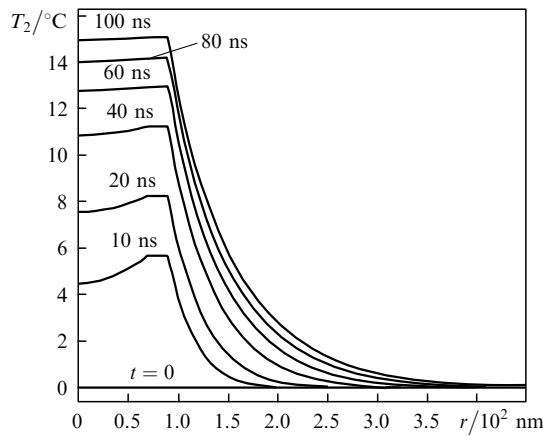
Figure 10. Distribution kinetics of the temperature T_2 along the radial coordinate in the microscopic domain 'composite nanoparticle and its neighbourhood' during the 100-ns pump pulse.

Figure 12. Image of a nanoshell after its destruction by a laser pulse, obtained by means of transmission electron microscopy. Adopted from [22].

Accepting the value of $1\,°C$ to be a significance test of the temperature increment, for the considered nanoparticles the limiting pulse duration will be $t_p^{lim} = 20$ ns, as follows from the analysis of curves in Fig. 10. The reduction of the pulse duration below t_p^{lim} with a simultaneous increase in the intensity I leads to a considerable spatial inhomogeneity of the temperature field during the whole time of action of the irradiating pulse. This is represented in Fig. 11, where the results of calculation for the pulse duration of 1 ns are displayed.
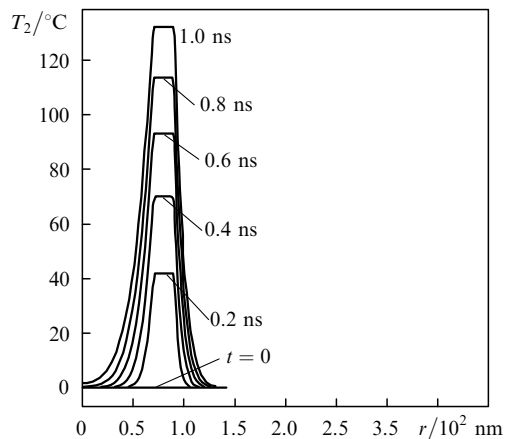
nanoparticles [22], not yet interpreted physically, namely, the melting of the shell and the formation of liquid gold drops on the core of the nanoparticle (Fig. 12).

4. Conclusions

Based on the two-scale modelling presented, the characteristic features of time-dependent temperature fields, formed in media with absorbing nanoparticles, are investigated. The proposed technique of using the effects of the absorbed laser radiation power localisation and the algorithms for calculating the parameters of spatiotemporal thermal action seem promising for synthesis and development of computerised systems, providing the level estimation and the adaptive control of the processes of dosing hyperthermia of relatively large regions of biotissue, as well as of separate cells (e.g., at the injection of a certain absorber directly into the tumour tissue, or at the accumulation of functionalised nanoparticles in the tumour tissue under systemic administration).

Figure 11. Distribution kinetics of the temperature T_2 along the radial coordinate in the microscopic domain 'golden nanoshell and its neighbourhood' during the 1-ns pump pulse.

A considerable time delay is clearly seen between the heating of the major part of the core material and that of the golden shell of the nanoparticle, and by the end of the pulse the corresponding temperature difference within the nanoparticle reaches the value of $\sim 130\,°C$.

The essential inhomogeneity of the temperature distribution inside a composite nanoparticle in the course of the pulses with $t_p < t_p^{lim}$ allows one to predict the possibility of shell melting before the core of the nanoparticle could heat up to the softening temperature of the core material. The result found by numerical calculations explains the experimentally observed picture of destruction of composite
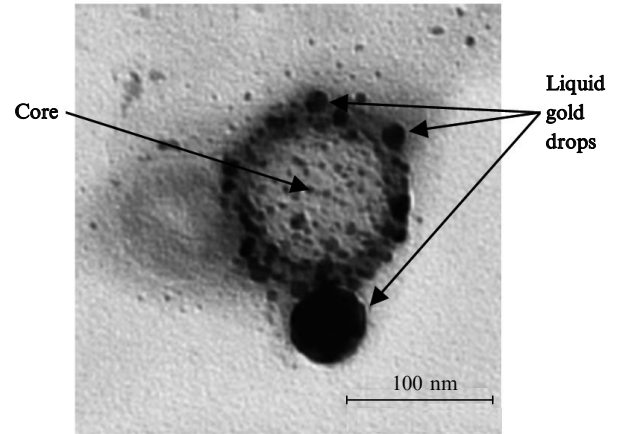
Appendix

As well known (see, e.g., [15]), the quantity β used above and proportional to the ratio of the energy density of the electric field, diffracted into the shell of a nanoparticle, to that of the irradiating field in the surrounding medium, may be easily found within the framework of quasi-electrostatic approximation:

$$\beta \equiv \frac{|E_2|^2}{|E_m|^2} = |C|^2 + \frac{1 - 3\cos^2\theta}{r^3} 2\mathrm{Re}(DC^*)|$$

$$+ \frac{1 + 3\cos^2\theta}{r^6} |D|^2, \tag{A1}$$

$$C = \frac{-3\varepsilon_m(\varepsilon_1 + 2\varepsilon_2)}{\Delta}, \quad D = \frac{3\varepsilon_m(\varepsilon_1 - \varepsilon_2)R_1^3}{\Delta},$$

$$\Delta = (\varepsilon_1 + 2\varepsilon_2)(\varepsilon_2 + 2\varepsilon_m) + 2\left(\frac{R_1}{R_2}\right)^3 (\varepsilon_1 - \varepsilon_2)(\varepsilon_2 - \varepsilon_m).$$

Here, E_m is the complex electric-field amplitude of the electromagnetic wave, propagating in the medium and linearly polarised in the direction of the vector $\boldsymbol{v}$; θ is the angle between this vector and the direction vector pointing at the observation point located at the distance r ($R_1 \leqslant r \leqslant R_2$) from the centre of a spherical nanoshell; $\varepsilon_j = n_j^2$ are the dielectric constants of the corresponding media ($j = 1$, 2, m).

In the case $|\varepsilon_2| \gg |\varepsilon_1|, |\varepsilon_m|$ for relatively thin shells ($R_2 - R_1 \ll R_1$), the expression for the quantity β can be essentially simplified, and Eqn (A1) yields the following rough estimate

$$\beta(\theta) \approx \frac{9}{4} |C|^2 \sin^2 \theta. \qquad (A2)$$

The elementary averaging of Eqn (A1) over the volume of the nanoparticle shell $V_{cov} = 4\pi(R_2^3 - R_1^3)/3$ yields the expression

$$\langle \beta \rangle \equiv V_{cov}^{-1} \int_{V_{cov}} \mathrm{d}^3 \boldsymbol{r} \beta = |C|^2 + \frac{2}{(R_1 R_2)^3} |D|^2. \qquad (A3)$$

References

1. Müller G., Roggan A. (Eds) *Laser-Induced Interstitial Thermotherapy* (Bellingham, WA: SPIE Press, 1995).
2. Bagratashvili V.N., Sobol E.N., Shekhter A.B. (Eds) *Lazernaya inzheneriya khryashchei* (Laser Engineering of Cartilages) (Moscow: Fizmatlit, 2006).
3. Tuchin V.V. *Tissue Optics: Light Scattering Methods and Instruments for Medical Diagnosis* (Bellingham, WA: SPIE Press, 2007).
4. Shcherbakov Yu.N., Yakunin A.N., Yaroslavsky I.V., Tuchin V.V. *Opt. Spectrosk.*, **76**, 845 (1994).
5. Shcherbakov Yu.N., Yakunin A.N., Yaroslavsky I.V., Tuchin V.V. *Opt. Spectrosk.*, **76**, 851 (1994).
6. Terentyuk G.S., Maslyakova G.N., Suleymanova L.V., Khlebtsov N.G., Khlebtsov B.N., Akchurin G.G., Maksimova I.L., Tuchin V.V. *J. Biomed. Opt.*, **14** (2), 021016 (2009).
7. Terentyuk G.S., Maslyakova G.N., Suleymanova L.V., Khlebtsov B.N., Kogan B.Ya., Akchurin G.G., Shantrocha A.V., Maksimova I.L., Khlebtsov N.G., Tuchin V.V. *J. Biophoton.*, **2**, 292 (2009).
8. Richardson H.H., Carlson M.T., Tandler P.J., Hernandez P., Govorov A.O. *Nano Lett.*, **9**, 1139 (2009).
9. Ratto F., Matteini P., Rossi F., Menabuoni L., Tiwari N., Kulkarni S.K., Pini R. *Nanomedicine: Nanotechnology, Biology, and Medicine*, **5**,143 (2009).
10. Khlebtsov N.G. *Kvantovaya Elektron.*, **38**, 504 (2008) [*Quantum Electron.*, **38**, 504 (2008)].
11. Letfullin R.R., George T.F., Duree G.C., Bollinger B.M. *Adv. Opt. Technol.*, Article ID 251718 (2008).
12. Girard C., Dujardin E., Baffou G., Quidant R. *New J. Phys.,* **10**, 105016 (2008).
13. Avetisyan Yu.A., Yakunin A.N., Tuchin V.V. *Digest of Workshop on Laser Physics and Photonics XI (SFM'09)* (Saratov, Russia, 2009).
14. Avetisyan Yu.A, Yakunin A.N., Tuchin V.V., in *Abstracts of Scientific-Practical Conference 'Nanotechnologies to Industry-2009''* (Fryazino, Russia, 2009) p. 69.
15. Bohren C.F., Huffman D.R. *Absorption and Scattering of Light by Small Particles* (New York: Wiley, 1998).
16. Buffat Ph., Borel J.-P. *Phys. Rev.*, **13**, 2287 (1976).
17. Rezchikov A.F., Yakunin A.N. *Konechno-elementnoe modelirovanie ob'ektov pretsizionnogo priborostroeniya pri silovykh i tepolovykh vozdeistviyakh* (Finite-Element Modelling of the Objects of Precision Instrument Engineering under the Force and Thermal Actions) (Saratov: Izdatelskii tsentr 'Nauka', 2008).
18. Vladimirov V.S. *Uravneniya matematicheskoi fiziki* (Equations of Mathematical Physics) (Moscow: Nauka, 1976).
19. Landau L.D., Lifshitz E.M., Pitaevskii L.P. *Electrodynamics of Continuous Media* (Oxford: Butterworth-Heinemann, 1984).
20. Zimmerman W.B.J. *Multiphysics Modeling with Finite Element Methods* (New Jersy – London – Singapore: World Scientific Publ. Comp., 2006).
21. Isachenko V.P., Osipova V.A., Sukomel A.S. *Teploperedacha* (Heat Transfer) (Moscow: Mir Publishers, 1969).
22. Akchurin G., Khlebtsov B., Akchurin G., Tuchin V., Zharov V., Khlebtsov N. *Nanotechnol.*, **19**, 015701 (2008).